EC MODELLING AND ENHANCEMENT SIGNALS IN CFRP INSPECTION

G. Megali, D. Pellicanò, M. Cacciola, S. Calcagno M. Versaci and F. C. Morabito

DIMET Department
University "Mediterranea" of Reggio Calabria
Via Graziella Feo di Vito, I-89100 Reggio Calabria, Italy

Abstract—Non Destructive Testing techniques are more and more exploited in order to quickly and cheaply recognize flaws into the inspected materials, specially for carbon fiber reinforced polymers in recent years. Their production which are widely used both in civil and military applications, is an elaborate process un-free from faults and problems. Problems during the manufacturing, such as plies' overlapping, can cause flaws in the resulting material, this way compromising its integrity. Within this framework, this work aims to propose a design of ferrite core probe for eddy current non destructive evaluation, in order to investigate the presence of defects in carbon fiber epoxy composite materials. In this context, modelling is a powerful tool for inspection improvements. It helps probe-coil designers to optimize sensors for each examination requirement, providing better understanding of the involved physics, supporting operator training and increasing defect analysis reliability. Particularly, Finite Element based analyzes will be carried out into this path. After this step, in order to improve the quality of simulated measurement, a filtering technique has been exploited in order to improve the accuracy and performance of the flaw detection.

1. INTRODUCTION

In order to improve manufacturing quality and ensure public safety, components and structures are commonly inspected for early detection of defects or faults which may reduce their structural integrity. Non Destructive Technique and Evaluation (NDT&E), particularly

Eddy Current Testing (ECT), present the advantage of leaving the specimens undamaged after inspection [1]. Within this framework, EC inspection of composite materials is of importance in many domains of industry: energy production (nuclear plants), transportation (aeronautic), workpiece manufacturing, and so forth. This technique, based on the investigation of magnetic flux of exciting coils placed close to the specimen under analysis, is used to detect and characterize possible flaws or anomalies in specimens. NDT&E of advanced composites materials offers an exciting and interesting challenge to both researchers and applied technologists [2]. Unlike NDE homogenous materials NDE, where interest is focused on detection, location, orienting and sizing of single cracks, NDE state-of-art in composites is presently in detecting a variety of damage modes [1, 3]. Hence, it is still not possible to suggest to NDT personnel exactly what type of damage, size, orientation, etc. needs to be found in an inspection process. So, the challenge. Challenging for researchers in the area of NDE of composites is in the fact that nondestructive evaluation is presently playing an important role in helping to identify damage in the final failure process. In this way, materials can be inspected by using ECTs [4, 5]. In contrary to the traditional targets of the EC investigations, the carbon fibre reinforced plastic materials (CFRPs) has non isotropic and non continuous but patterned spatial distribution of the conductivity due to the composite structure [6–8]. Therefore, the study as well as the modelling of the interaction between the composite materials and the electromagnetic field requires novel approach [9]. The method of approach depends on the objectives of the investigation. Typical testing configurations may consist of ferrite core coil probes, placed above a planar (or at least locally planar) composite specimen and operating at frequency depending on the problem (typically between a few Hz to a few MHz) [10]. The aim of ferrite core is to focus the magnetic flux into the certain area of the specimen, in order to increase the probe sensitivity to the defect. For each application, the coil model, as well as, the operating frequencies are set according to the task. This paper proposes an application of a novel electromagnetic computational method for the problem of ferrite core based EC probe can be used for inspecting of CFRPs. For our purpose a Finite Element Method (FEM) based software has been exploited in order to optimize the sensor effect and the drop-in suppression, the operating parameters of the frequency and field strength and for geometrical and physical modelling [11]. In order to simulate the response of a probe to the presence of defects, it is necessary to study how a probe excites the specimen to be tested, considering its electrical anisotropy. Usually, the goal is the

optimization of probe and the assessment of such perturbation as lift-off and tilting. In the investigated situation, the probe is placed above and parallel to a composite block. It is made of a E-profiled ferrite core, excited by a coaxial coil. We verify the variation of voltage ([V]) with respect on linear scanning direction. In our FEM, since we use $\mathbf{A} - \psi$ formulation, just the z-component of magnetic potential $\mathbf{A}$ is non null. Finally, EC map has been processed with an Adaptive Homomorphic Filtering (AHF) [12] in order to improve the interpretability or the perception of information in images for human viewers or to provide the 'better' input for the other automated image processing techniques. This paper presents the details and numerical results of our study. It is organized as follows: firstly, a brief description of CFRP is treated, considering their electrical properties; than, the exploited approach and some important results are displayed and, finally, some conclusions are drawn.

2. INTRODUCTION ABOUT COMPOSITE MATERIALS

CFRP are composites made with carbon fibers embedded in a polymer, commonly epoxy matrix. To form a composite sheet, carbon fibers are immersed in a thin layer of resin. Several layers are then assembled together with different fiber orientations to achieve the required thickness and the mechanical strength. The fibers, which are usually 7 to 15 μm in diameter [13], are bundled together to form a tow, which can then be woven into a fabric or laid down unidirectionally to form a lamina. A single lamina having a thickness of about 0.05–0.2 mm, in order to build mechanical components having improved structural properties, many laminate are stacked in same or different directions to form a laminate (as shown in Fig. 2.) This fiber directionality contributes to the electrical anisotropy in CFRP which means the composite conductivity is typically much higher along the fiber direction and lower perpendicularly [14]. Because of their heterogeneous composition, composites present a combination of properties otherwise unavailable through the use of more conventional materials. The manufacture of composite materials is still expensive as it is a labor intensive production process which requires sophisticated equipment. Despite their advantages, the materials show relatively poor resistance to impact and ageing. In order to carry out NDT characterization of CFRP structures and optimize their manufacturing, different inspection techniques have been studied and developed such as ultrasonic tests, scanning acoustic microscopy, embedded optical fibre, microwave technique scanning and DC or AC conductivity measurements. ECT has gained interest for in-service inspection and
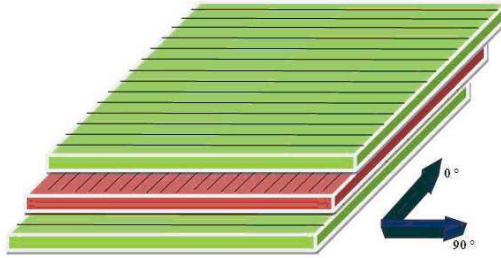
Figure 1. Example of representation of CFRP structure.

rapid quality control thanks to its simplicity, and specimen — probe non-contacting [15].

The limited understanding of composites and their complex failure mechanisms present problems in establishing safety limits. Composite materials are used in a wide range of industries, including aerospace, transport and leisure, in the manufacture of aircraft, trains, cars and sports equipment such as golf clubs and tennis rackets. Composite materials combine the advantages of high strength, high fatigue resistance, good thermal oxidative stability, freedom of design and very low weight compared to more conventional materials such as aluminium or steel. For these reasons they are now extensively used, but there is limited knowledge concerning the effect of impact damage, delamination and fatigue cycling on the mechanical properties of composites. In order to meet safety criteria required by industries, composites need to be carefully inspected to assess for structural integrity. The heterogeneous and multi-layered characteristics (see Fig. 1) of these materials make them difficult to inspect with conventional NDTs. At the present time, there is an increasing need for efficient and accurate NDTs.

2.1. Carbon Fiber Electrical Properties

In this section a characterization of electromagnetic properties of CFRP materials is proposed; it exhibits [7] a linear relationship between its electrical resistivity and $\sin^2(\theta)$, where θ is the angle between the nominal lay of fibers and the x-axis (see Fig. 2).

Carbon fibers have a intrinsic electrical conductivity; therefore, one might expect that the CFRP material made from these fibers would be electrically conductive in the direction of the fibers. In addition, a significant transverse electrically conductivity is also observed as result of a tight fiber-to-fiber contact. Whereas the longitudinal
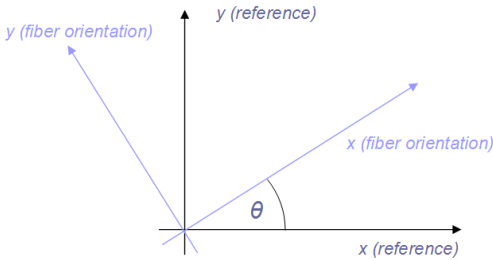
Figure 2. Relation between the principal axes, reference axes, and fiber orientation.
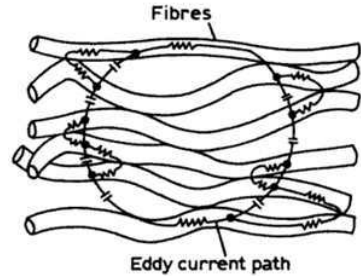
Figure 3. Resistive reactive eddy current path.

conductivity increases linearly with the fiber volume fraction, the transverse conductivity increases with the fiber volume fraction in a more complicated scaling relationship. The electrical anisotropy depends on the volume fraction of the material; hence, the longitudinal conductivity varies between 5×10^3 and 5×10^4 S/m the transverse conductivity ranges between 10 and 100 S/m. When the unidirectional layers are composed in a cross-ply to build a composite plate, there is a onset of a cross-ply conductivity [7], equal to 7633 S/m. Another peculiarity of these materials concerns the trend of currents induced by a ferrite core probe: they exhibit an elliptical pattern caused by the anisotropy (see Fig. 7). Usually, the EC path in an unidirectional CFRP is partially resistive along fibers, and partially capacitive across resin, jumping among fibers. At low test frequencies, the reactance of the capacitive path becomes appreciably high, and a current path across the resin matrix becomes an unfavorable one. Consequently, ECs flow along fibers and from one fiber to another at the points of fiber-fiber contact (the well-known "resistive path"). At higher frequencies (typically [MHz]), the inter-fiber reactance (i.e., the reactance across the resin matrix) becomes comparable to the resistance along the single lamina. Consequently, an eddy current path which is resistive-capacitive, as shown in Fig. 3 [16], better describes the electrical characterization of the laminate.

3. FEM APPROACH

The problem of analyze a CFRP specimen using EC by analytical method is rather complex. For this reason a numerical approach is indicated [11]. Particularly, in this section of the paper, we want to show how the behavior of a ferrite core EC probe can be simulated

in order to detect defects in CFRPs. The simulations exploit a FEM and require geometrical and physical definition of the same coil, its ferrite core and the CFRP plate. The exciting current, i.e., I_{eff}, and the frequency, i.e., f_{exc}, have been varied according to the skin-effect phenomenon, in order to evaluate the simulation results. For our purpose, we verified the variation of output voltage ([V]) when the probe moves right over the surface of the specimen. The numerical technique proposed exploits a FEM code and the 3D $\mathbf{A} - \Psi$ formulation [17]. In a general subdomain Ω, the magnetic potential $\mathbf{A}$ is obtained by:

$$-\nabla \cdot \left(j\omega\sigma - \omega^2\epsilon_0\epsilon_r \right) \mathbf{A} - \sigma\mathbf{v} \times (\nabla \times \mathbf{A}) + (\sigma + \omega\epsilon_0\epsilon_r) \nabla V - \mathbf{J^e} = 0 \quad (1)$$

$$\left(j\omega\sigma - \omega^2\epsilon_0\epsilon_r \right) \mathbf{A} + \nabla \left(\mu_0^{-1}\mu_r^{-1}\nabla \times \mathbf{A} \right) - \sigma\mathbf{v} \times (\nabla \times \mathbf{A})$$
$$+ (\sigma + \omega\epsilon_0\epsilon_r) \nabla V = \mathbf{J^e} \quad (2)$$

where σ is the conductivity; ω is the angular pulsation; μ_0 and μ_r are free space and relative magnetic permeability respectively; ϵ_0 and ϵ_r are the free space and relative permittivity respectively; are the void's and the material's dielectric constants, respectively; $\mathbf{v}$ is the instantaneous velocity of the object derived from the expression of the Lorentz force and $\mathbf{J^e}$ is the external current density on the exciting coil. Since the object is fixed, $\mathbf{v} = 0$. Please consider that $\nabla\cdot$ and $\nabla\times$ represent respectively the divergence and rotor differential operators expressed by the nabla operator. In order to set point-by-point $\mathbf{J^e}$, we used the direction cosine trigonometric formulation [17]:

$$J_{0,x} = -\frac{J_0 \cdot \hat{y}}{\sqrt{(\hat{x}^2 + \hat{y}^2)}}; \quad J_{0,y} = -\frac{J_0 \cdot \hat{x}}{\sqrt{(\hat{x}^2 + \hat{y}^2)}} \quad (3)$$

where $\hat{x}$ and $\hat{y}$ are the coordinates of outer points of the coil; J_0 is the density of current inside copper volume. In detail:

$$J_0 = \left(\frac{I_0}{2\pi\sqrt{(\hat{x}^2 + \hat{y}^2)}} \right) h_{coil}; \quad I_0 = I_{\max}\sin(\omega t); \quad I_{\max} = I_{eff}\sqrt{(2)} \quad (4)$$

$J_{0,x}$ and $J_{0,y}$ have been computed by the resolution of a trigonometric problem, the so-called direction cosine so that the current has a tangent value (see Fig. 4 for details).

In particular, in this application it is possible to write:

$$\cos\alpha = -\sin\gamma = -\frac{\hat{y}}{\sqrt{(\hat{x}^2 + \hat{y}^2)}}; \quad \sin\alpha = \cos\gamma = \frac{\hat{x}}{\sqrt{(\hat{x}^2 + \hat{y}^2)}} \quad (5)$$

(please refer to Fig. 4 for α and γ angles representation). The ferrite core probe has been modelled according to [18, 19]. In our FEM code, boundary conditions were set as follows: magnetic insulation ($\mathbf{n} \times \mathbf{A} = 0$ derived from $\mathbf{B} \cdot \mathbf{n} = 0$), for fictitious subdomain
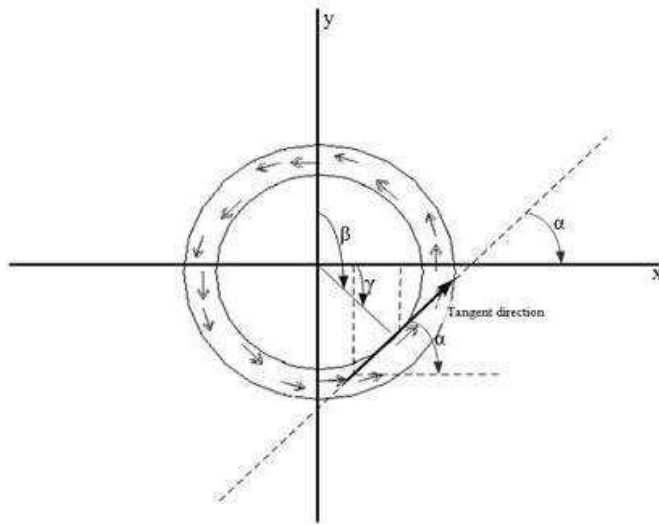
Figure 4. Computation of density of current by means of direction cosine.

(representation of an infinite volume) [20] whereas the continuity for the CFRP specimen is insured by $\mathbf{n} \times (\mathbf{H}_1 - \mathbf{H}_2) = 0$ [20]. Our simulations have been based on a discrete domain [21] having 17287 elements. Mesh has been generated with tetrahedral elements (size of 0.05 mm) for the CFRP plate, the exciting coil and its ferrite core. The composite plate [90°, 0°, 90°] (sizes 7 cm × 5 cm × 1.8 mm) has been modelled with three parallelepipeds representing three different layers. The conductivity of the CFRP plate is given by the following expression:

$$[\sigma] = [R]^{-1} \cdot [\sigma'] \cdot [R] \tag{6}$$

where $[R]$ is a rotation matrix which relates the components in the primed coordinate system to the unprimed coordinate system (see Fig. 2). Respectively, $[R]$ and $[\sigma']$ are equal to:

$$[R] = \begin{bmatrix} \cos\theta & -\sin\theta & 0 \\ \sin\theta & \cos\theta & 0 \\ 0 & 0 & 1 \end{bmatrix} \tag{7}$$

$$[\sigma'] = \begin{bmatrix} \sigma_l & 0 & 0 \\ 0 & \sigma_t & 0 \\ 0 & 0 & \sigma_{cross} \end{bmatrix} \tag{8}$$

where σ_l is the conductivity along the fibers, σ_t is the conductivity transverse to the fiber orientation and σ_{cross} is the conductivity with

(a) Fiber orientation: 0 Degrees   (b) Fiber orientation: 90 Degrees
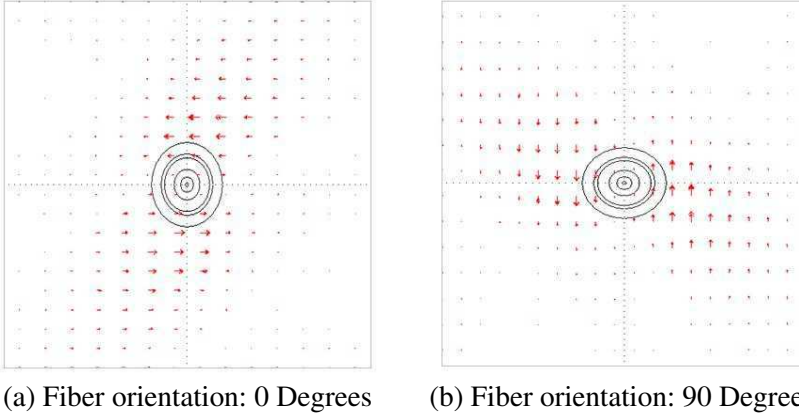
Figure 5. X-Y plane: Eddy current distribution for various fiber orientations.

overlapping of unidirectional layers [22]. These reference axes, along with the conductivity matrix is diagonal, are considered the principal axes. When the fibers are oriented at some arbitrary angle θ (as shown in Fig. 2) with respect to the x-axis, the conductivity matrix is no longer diagonal and there is cross coupling of the components. Fig. 5 illustrates the eddy currents distribution for two fiber orientations.

4. SIMULATIONS AND EXPERIMENTATIONS

A number of simulations have been carried out with different values of frequency f_{exc}, current I_{eff} and size of the defect, according the general representation shown in Fig. 6. Numerical simulations refer to two cylindrical defect with a basis diameter equal to 10 mm. Please note the evident variation of voltage for defects presence (see Fig. 9 for details). Simulations carried out by FEM approach have been exploited to build a new exciting ferrite core probe coil for detecting cylindrical defects in CFRP by means of Giant MagnetoResistive (GMR) sensor [23]. What one should wait when moving from simulations to in-lab measurement is the voltage increase is smaller, due to a number of factors, such as the geometry of the defect no longer referable as a perfect cylinder.

Figure 9 shows the comparison between a numerical simulation and in-lab measurement with a $f_{exc} = 15$ kHz and a $I_{eff} = 100$ mA for defects' detection of proposed specimen. In order to map the interesting area, the ferrite core probe coil has been moved over the specimen by means of a 0.5 mm step-by-step automatic scanning. The
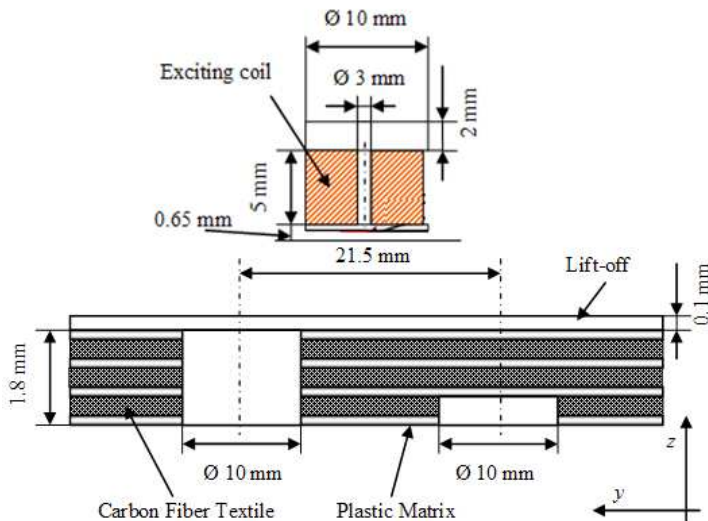
Figure 6. Measurement set-up for defect (hole) detection: detection of 100% and 33% deep Ø 10 mm holes from opposite (OD defect) and from defect side (ID defect).
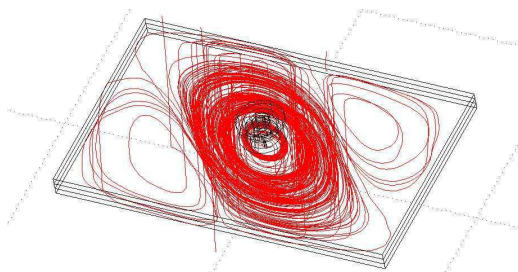
Figure 7. Elliptical pattern for the induced currents.

probe has been designed and fabricated based upon the proposed exciting system to evaluate its efficiency and benefits (see Fig. 8).

During our in-lab measurements, frequency f_{exc} and current I_{eff} have been varied according to the simulations. The performances of our new ECT probe have been evaluated and the design of new exciting system assures the detection of defects according to the magnitude of electrical parameters (exciting frequency and current) imposed in FEM simulation.

Subsequently, bi-directional inspections have been carried out in
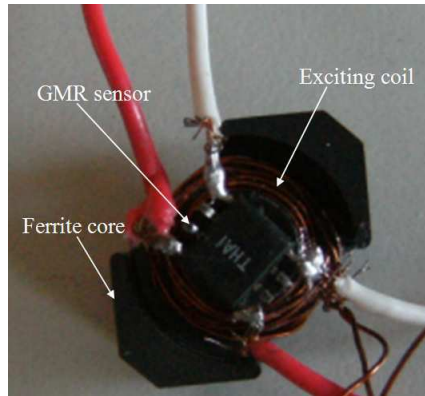
Figure 8. GRM, coil and Ferrite-core for GMR-ECT probe.
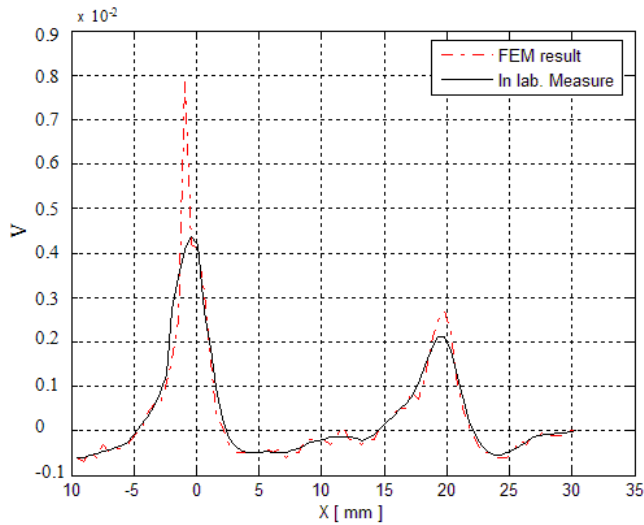
Figure 9. Variation of voltage with respect on linear scanning direction.

order to obtain EC map characterized by defects' presence (please refer to Fig. 12, on the left).

5. AHF FOR ENHANCING EC MAP

The aim of image enhancement is to improve the interpretability or the perception of information in images for human viewers or to provide

the 'better' input for the other automated image processing techniques. But, unfortunately there is no general rule or any mathematical criterion for determining what is 'good' image enhancement when it comes to the human perception. If the image looks good, it is good. This section considers the homomorphic filtering for the measurement of the degree of the enhancement of images in NDT&E. Classical theory about filtering makes use of linear filters for the improvement of Signal-to-Noise Ratio (SNR). Our implementation regards a non-linear system based on a generalized principle of linearity. White and black images can be represented by means of a 2-variable system. Images are composed by reflection of the light from physical objects. The process of realization of an image can be modelled like a product about a lighting (f_i) and a reflection (f_r) function [12]:

$$f(x,y) = f_i(x,y) \cdot f_r(x,y) \tag{9}$$

This equation cannot be used to operate separately on the frequency components of illumination and reflectance directly because the Fourier transform of the product of the functions is not separable. So, Equation (9) can not be expressed as:

$$\Im f(x,y) = \Im f_i(x,y) \cdot \Im f_r(x,y) \tag{10}$$

but if image $f(x,y)$ can be defined as follows $\Im z(x,y) = \Im \ln f(x,y) = \Im \ln f_i(x,y) + \Im \ln f_r(x,y)$ or

$$Z(u,v) = F_i(u,v) + F_r(u,v) \tag{11}$$

where, $F_i(u,v)$ and $F_r(u,v)$ in Equation (11) are the Fourier transforms of the terms defined earlier $\ln f_i(x,y)$ and $\ln f_r(x,y)$ [12]. The function
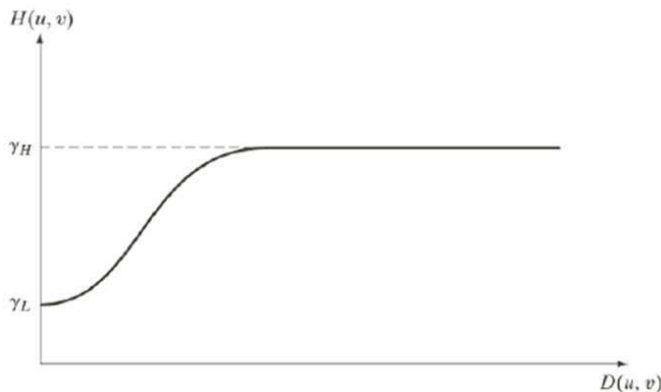
Figure 10. Cross-section of Homomorphic filter function.

$Z(u, v)$ can be processed by means of a filter function $H(u, v)$ and can be expressed as

$$S(u, v) = H(u, v) \cdot Z(u, v) = H(u, v) \cdot F_i(u, v) + H(u, v) \cdot F_r(u, v) \quad (12)$$

where $S(u, v)$ is the Fourier transform of the result. In the spatial domain $s(x, y) = \Im^{-1} S(u, v) = \Im^{-1} H(u, v) \cdot F_i(u, v) + \Im^{-1} H(u, v) \cdot F_r(u, v)$ by letting $f'_i(x, y) = \Im^{-1} H(u, v) \cdot F_i(u, v)$. Finally the equation becomes

$$s(x, y) = f_i(x, y) + f_r(x, y) \quad (13)$$

and

$$g(x, y) = e^{s(x,y)} = e^{f_i(x,y)} + e^{f_r(x,y)} = f_{i0}(x, y) \cdot f_{r0}(x, y) \quad (14)$$

where $f_{i0}(x, y) = e^{f'_i(x,y)}$ and $f_{r0}(x, y) = e^{f'_r(x,y)}$ are the illumination and the reflectance components of the output image. This method is based on a special case of class of systems known as Homomorphic system. The filter transfer function $H(u, v)$ is known as the Homomorphic filter function:

$$H(u, v) = \gamma_L + \frac{\gamma_H}{1 + \left[\frac{D_0}{\sqrt{(u^2+v^2)}} \right]^{2n}} \quad (15)$$

where γ_L, γ_H are the lower and the higher frequency components respectively, D_0 is the cut-off frequency and n defines the order of the filter. A good choice between the lower and the higher frequency provides a dynamic range of the compression and enhancement [12]. $H(u, v)$ acts on the illumination and the reflectance components of the input image separately. The illumination component of an image is generally characterized by the slow spatial variations while the reflectance components vary abruptly, particularly at the junctions of dissimilar objects. These characteristics actually lead to associate the low frequencies of the Fourier transform of the logarithm of an image with illumination and the high frequencies with reflectance [24]. This process of enhancement can be expressed by using the block diagram shown in Fig. 11. Homomorphic filters use the Discrete Fourier Transforms (DFT) as the core transform. Presently, in digital images, more efficient tool for transformations are used, such as Fast Fourier Transform (FFT) [25, 26]. Homomorphic filter helps to have a good control over the illumination and the reflectance. In our algorithm, for a homomorphic filter of order 2, the cut-off frequency D_0 is adaptively calculated by inspecting the Fourier Spectrum of the considered image and finding the maximum value of the spectrum. Then, we calculate the highest frequency showing a 3 dB loss as the final cut-off frequency. The inputs of our processor are: the image to be filtered (img); the

order of the Homomorphic filter is 2 (in our case, $n = 1$). The output are the filtered image (img_f). A visual comparison of the proposed approach is shown in Fig. 12.
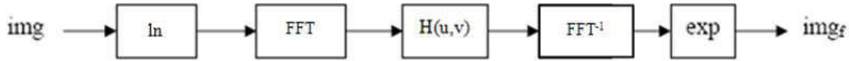
Figure 11. Block diagram of the AHF.
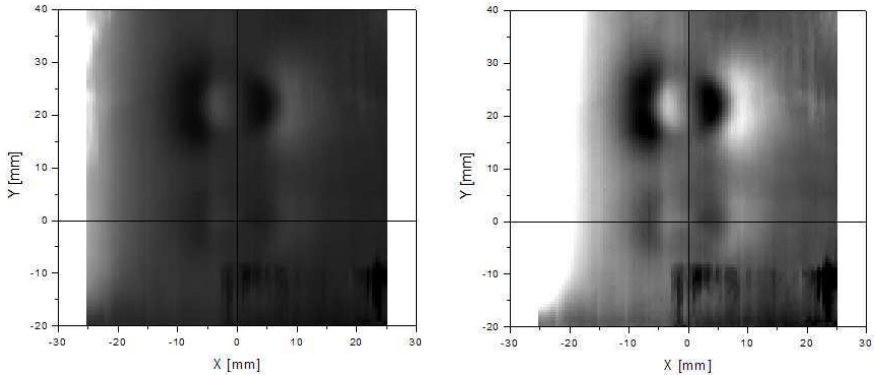
Figure 12. Results on defects at 15 kHz: (on the left) $|B_x|$; (on the right) enhanced view of $|B_x|$.

6. CONCLUSION

In this paper, an implementation of ferrite cored EC probe for detection of defects in composite materials is presented. Based on numerical simulations carried out with a FEM based approach, ECs and voltage variations during the inspection have been investigated. For the implementation of ferrite core EC probe, a time-harmonic FEM code with 3-D geometries has been studied to evaluate defects presence. The in-lab measurements confirmed the results obtained by FEM simulations, so the proposed method provides a good overall accuracy in detecting defects' presence, as our comparison demonstrate. Moreover, to obtain the enhanced performance in the EC map processing, an AHF approach has been exploited. In order to enhance the improvement of the interpretability or the perception of information in images for human viewers or to provide the 'better' input for the other automated image processing techniques.

Unfortunately there is no general rule or any mathematical criterion for determining what is 'good' image enhancement when it comes to the human perception. If the image looks good, it is good. It is also true for the converse idea. Within this framework, before applying the proposed approach of the EC map enhancement in practical purposes, further investigations will be made. Further work suggests the possibility to test and compare our algorithm to a large range of measurements, on the basis of the evaluation of performance (i.e., SNR analysis). At the same time, considering the FEM approach, the procedure should be validate for defects with different shape or for different ferrite core probe profiles. The authors are actually engaged in this direction.

REFERENCES

1. Yamada, S., M. Katou, M. Iwhara, and F. P. Dawson, "Eddy-current testing," *IEEE Trans. Magn.*, Vol. 31, No. 6, 3185–3187, 1995.
2. Balanis, C. A., *Advanced Engineering Electromagnetics*, John Wiley & Sons, New York, 1995.
3. Nevadunsky, J. J., "Early fatigue damage detection in composite materials," *J. Comp. Mater.*, Vol. 9, 394–408, 1975.
4. De Goeje, M. P. and K. E. D. Wapenaar, "Non-destructive inspection of carbon fiber-reinforced plastics using eddy current methods," *Composites*, Vol. 23, No. 9, 147–157, 1992.
5. Lange, R. and G. Mook, "Structural analysis of CFRP using eddy current methods," *NDT&E International*, Vol. 27, No. 5, 241–248, 1994.
6. Knibbs, R. H., and J. B. Morris, "The effects of fiber orientation on the physical properties of composite," *Composites*, Vol. 5, No. 5, 209–218, 1974.
7. Valeau, A. R., "Eddy current nondestructive testing of graphite composite materials," *Mater. Eval.*, Vol. 48, 230–239, 1990.
8. Owston, C. N., "Eddy current methods for the examination of carbon fiber reinforced epoxy resins," *Mater. Eval.*, Vol. 34, 237–244, 1976.
9. Angelidis, N. E., N. Khemiri, and P. E. Irving, "Experimental and finite element study of the electrical potential technique for damage detection in CFRP laminates," *Smart Mater. Struct.*, Vol. 14, 147–154, 2005.
10. Theodoulidis, T. P., "Model of ferrite-cored probes for eddy-

current non-destructive evaluation," *J. Appl. Phys.*, Vol. 93, 3071–3078, 2003.

11. Cacciola, M., G. Megali, D. Pellicanò, S. Calcagno, M. Versaci, and F. C. Morabito, "Modelling and validating Ferrite-core probes for GMR-Eddy current testing in metallic plates," *PIERS Online*, Vol. 6, No. 3, 237–241, 2010.

12. Ponomarev, V. and A. Pogrebniak, "Image enhancement by homomorphic filters," *Proc. SPIE, Applications of Digital Image Processing XVIII*, A. Tescher, Ed., Vol. 2564, 153, 1995.

13. Briggs, A., "Review: Carbon fibre-reinforced cement," *J. Mater. Sci.*, Vol. 12, 384–404, 1977.

14. Veron, S. N., "A single-aided eddy current method to measure electrical resistivity," *Mater. Eval.*, Vol. 46, 1581–1589, 1988.

15. Moulder, J. C., E. Uzal, and J. H. Rose, "Thickness and conductivity of metallic layers from eddy current measurements," *Rev. Sci. Instrum.*, Vol. 63, 3455–3465, 1992.

16. Prakash, R., "Non-destructive testing techniques," New Age Science LTD, United Kingdom, 2009.

17. Cacciola, M., S. Calcagno, G. Megali, F. C. Morabito, D. Pellicanò, and M. Versaci, "FEA design and misfit minimization for in-depth flaw characterization in metallic plates with eddy current nondestructive testing," *IEEE Trans. Magn.*, Vol. 45, No. 3, 1506–1509, 2009.

18. Cacciola, M., S. Calcagno, G. Megali, D. Pellicanò, M. Versaci, and F. C. Morabito, "Eddy current modelling in composite materials," *PIERS Online*, Vol. 5, No. 6, 591–595, 2009.

19. Cacciola, M., S. Calcagno, G. Megali, D. Pellicanò, M. Versaci, and F. C. Morabito, "Numerical simulations on Eddy currents evaluation at high speed in CFRP," *Proceedings of the Third Euro Mediterranean Symposium on Advances in Geomaterials and Structures, AGS 2010*, Vol. 1, 217–227, 2010.

20. Tsuboi, H. and T. Misaki, "Three dimensional analysis of eddy current distribution by the boundary element method using vector variables," *IEEE Trans. Magn.*, Vol. 26, No. 2, 454–457, 1990.

21. Weissenburger, D. and U. R. Christensen, "A network mesh method to calculate eddy current on conducting surfaces," *IEEE Trans. Magn.*, Vol. 18, No. 2, 422–425, 1982.

22. Pratap, B. and W. F. Weldon, "Eddy currents in anisotropic composites applied to pulsed machinery," *IEEE Trans. Magn.*, Vol. 32, No. 2, 437–444, 1996.

23. Dogaru, T. and S. T. Smith, "Giant magnetoresistance-based

Eddy-current sensor," *IEEE Trans. Magn.*, Vol. 37, No. 5, 3836–3838, 2001.

24. Gonzales, R. C. and R. E. Woods, *Digital Image Processing*, Addison Wesley, 1993.

25. Gonzales, R. C. and R. E. Woods, *Digital Image Processing Using Matlab*, Addison Wesley, 1996.

26. Umbaugh, S. E., *Computer Imaging: Digital Image Analysis and Processing*, CRC Press, Florida, 2005.